Detection of Infiltrating Fibroblasts by Single-Cell Transcriptomics in Human Kidney Allografts

Hemant Suryawanshi
Rockefeller University
Hua Yang
Weill Cornell Medical College, New York, NY
Michelle Lubetzky
Weill Cornell Medical College, New York, NY
Pavel Morozov
Rockefeller University
Mila Lagman
Weill Cornell Medical College, New York, NY
Alicia Alonso
Weill Cornell Medical College, New York, NY
Carol Li
Weill Cornell Medical College, New York, NY
Catherine Snopkowski
Weill Cornell Medical College, New York, NY
Franco Mueller
Weill Cornell Medical College, New York, NY
John Lee
Weill Cornell Medical College, New York, NY
Darshana Dadhania
Weill Cornell Medical College, New York, NY
Steven Salvatore
Weill Cornell Medical College, New York, NY
Surya Seshan
Weill Cornell Medical College, New York, NY
Vijay Sharma
Weill Cornell Medical College, New York, NY
Manikkam Suthanthiran
Weill Cornell Medical College, New York, NY
Thomas Tuschl
Rockefeller University
Thangamani Muthukumar (mut9002@med.cornell.edu)
Weill Cornell Medical College, New York, NY

Research Article

Keywords: scRNA-seq, AK1, AK2, cell

DOI: https://doi.org/10.21203/rs.3.rs-138499/v1

Abstract

We tested the hypothesis that single-cell RNA-sequencing (scRNA-seq) analysis of human kidney allograft biopsies will reveal distinct cell types and states and yield insights to decipher the complex heterogeneity of alloimmune rejection. We selected 3 kidney biopsies from 3 individuals for scRNA-seq and processed them fresh using an identical protocol on the 10x Chromium platform; (i) HK: native kidney biopsy from a living donor, (ii) AK1: allograft kidney with transplant glomerulopathy and tubulointerstitial fibrosis, and worsening graft function, and (iii) AK2: allograft kidney after successful treatment of active antibody-mediated rejection. We generated 7217 high-quality single cell transcriptomes. Taking advantage of the recipient-donor sex mismatches, we determined that in AK1 with fibrosis, more than half of the kidney allograft fibroblasts were—unexpectedly—recipient-derived and therefore likely migratory and graft infiltrative, whereas in the AK2 without fibrosis, all the fibroblasts were donor-derived. Furthermore, AK1 was enriched by tubular cells that overexpressed profibrotic extracellular matrix genes. AK2, eight months after successful treatment of rejection, contained endothelial cells that expressed T-cell chemoattractant cytokines. In addition to these key findings, our analysis revealed unique cell types and cell states. Altogether, single cell transcriptomics yielded novel mechanistic insights for individualizing the care of transplant recipients.

Introduction

Molecular approaches complementing conventional histopathology have propelled precision transplantation medicine to the bedside [1–3]. Single-cell RNA-sequencing (scRNA-seq) has provided hitherto unavailable opportunity to study cell types and cell states at an unprecedented level of precision [4–6]. Our goal was to investigate the utility of single-cell RNA-sequencing (scRNA-seq) at an individual patient level to address important conundrums in clinical transplantation. Given the complex heterogeneity of alloimmune rejection, we tested the hypothesis that single cell transcriptomics—by enabling molecular phenotyping of the host infiltrating cells and donor parenchymal cells—will yield novel mechanistic insights for individualizing the care of transplant recipients.

Immune rejection of the allograft remains a significant challenge despite the use of potent immunosuppressive drugs [7–9]. Rejection episodes restrict the benefits of transplantation and has a documented negative effect on long-term kidney allograft survival[10]. Treatment of rejection is constrained by the limited therapeutic armamentarium focused predominantly on the adaptive arm of the immune system and despite improvement in clinical and laboratory parameters, seldom achieves histological remission [10,11]. Despite improvement in clinical and laboratory parameters following anti-rejection therapy, it is possible that allograft injury persists at a molecular level. It is tempting to speculate that effective treatment of the lingering immune injury may improve the long-term outcome of kidney transplant recipients. This, however, requires better understanding of the complex immune interactions between the recipient genome and the genome of the organ donor.

We studied two clinico-pathological scenarios: (i) chronic persistent tissue injury and worsening allograft function and (ii) resolved acute tissue injury following successful treatment of an episode of active antibody mediated rejection. These results were compared to the single-cell transcriptomes of cells isolated from a native kidney used for living-donor kidney transplantation. We resolved 12 clusters of major cell types at the first level of gene expression analysis, which were further resolved by analysis of subgroups. We identified 4 distinct fibroblast subpopulations differentially present in the biopsies and made the surprising finding that more than half of the kidney allograft fibroblasts in the biopsy with chronic persistent tissue injury were kidney-recipient rather donor-derived. We also identified tubular progenitor cells with profibrotic gene signature. Finally, the transcriptomes of endothelial cell subtypes provided additional insights into the anti-allograft response.

Results

Clinical characteristics and kidney biopsy specimens

A summary of the clinical characteristics of the healthy kidney donor and the two kidney transplant recipients is provided in Table 1. Briefly, biopsy HK was obtained from a healthy 40-year old living kidney donor. The recipient who received kidney from this healthy living donor had immediate graft function and normal/stable serum creatinine at 12 months after transplantation with no major infections or acute rejection. Biopsy HK was done at the operating room during the back-table preparation of the native kidney prior to its implantation in the recipient.

Table 1
Clinical characteristics of the three subjects whose kidney biopsies were used for scRNA-seq

Clinical Information	Kidney Biopsies[a]		
	Native Kidney	**Allograft Kidney #1**	**Allograft Kidney #2**
	[HK][b]	**[AK1 (TG w/ graft dysfunction)][c]**	**[AK2 (aABMR f/u)][d]**
Donor characteristics	Living	Living	Living
Living/Deceased	Sister	Cousin	Brother
Relation of the donor to recipient	40 years	49 years	28 years
Age at donation	Female	Male	Female
Gender	White	Hispanic	African American
Race/Ethnicity			
Recipient characteristics	50	51 years	29 years
Age at Transplant	Male	Female	Male
Gender	White	Hispanic	African American
Race/Ethnicity	Diabetic nephropathy	Lupus nephritis	Focal segmental glomerulosclerosis
Native kidney disease			
At the time of transplantation	1-haploidentical	1-antigen mismatch	1-haploidentical
HLA-ABDR matching	Negative	Negative	Negative
CDC cross match[e]	Not done	Donor and Auto B cell Positive[f]	Negative
Flowcytometry cross match	Not Detected	Not Detected	Detected
Donor-specific anti-HLA antibodies[g]	Class I – 0	Class I – 0	HLA Class I – 2573 against Cw5
Mean fluorescence intensity value	Class II – 0	Class II – 0	HLA Class II MFI – 0
Induction immunosuppression	Basiliximab	Thymoglobulin	Thymoglobulin
Maintenance immunosuppression	Tacrolimus/Mycophenolate	Tacrolimus/Mycophenolate/Prednisone	Tacrolimus/Mycophenolate

Clinical Information	Kidney Biopsies[a]		
	Native Kidney [HK][b]	Allograft Kidney #1 [AK1 (TG w/ graft dysfunction)][c]	Allograft Kidney #2 [AK2 (aABMR f/u)][d]
From transplantation to index biopsy[h]		No	No
Delayed graft function		No	No
BK virus/ Cytomegalovirus viremia		1	1
Number of biopsies prior to index biopsy		26 months	76 months
Time, transplant to prior biopsy		1.11	2.16
Serum creatinine at prior biopsy, mg/dl		1.2	0.97
Urine albumin:creatinine ratio at prior biopsy, mg/g		Severe microvascular inflammation	Active antibody-mediated rejection
Prior biopsy findings		Severe transplant glomerulopathy	No transplant glomerulopathy
Prior biopsy Banff lesion scores[k]		No tubulointerstitial fibrosis[i]	No tubulointerstitial fibrosis[j]
Donor-specific anti-HLA antibodies at prior biopsy		g3, ptc2, i0, t0, cg3, cptc0, ci0, ct0, C4d-	g3, ptc3, i1, t0, cg0, cptc0, ci0, ct0, C4d+
Mean fluorescence intensity value		Not Detected	Detected
		Class I – 0	Class I – 2760 against Cw5
		Class II – 0	Class II – 17672 against DQ4
Index biopsy used for scRNA-seq[h]	0 months (at donation)	42 months	84 months
Time, transplant to index biopsy	No inflammation	Tacrolimus/Mycophenolate/	Tacrolimus/Mycophenolate/
Maintenance immunosuppression	No tubulointerstitial fibrosis	Prednisone	Prednisone
Time, prior biopsy to index biopsy	g0, ptc0, i0, t0, v0,	16 months	8 months
Serum creatinine, mg/dl	cg0, cptc0, ci0, ct0, C4d-	2.63	1.69
Serum tacrolimus trough, ng/dl		4.6	7.8
Urine albumin:creatinine ratio, mg/g		4.8	0.22
Index biopsy findings		Severe microvascular inflammation	Mild microvascular inflammation
Index biopsy Banff lesion scores[k]		Severe Transplant glomerulopathy	No Transplant glomerulopathy
Donor-specific anti-HLA antibodies at index biopsy		Moderate tubulointerstitial fibrosis[l]	No tubulointerstitial fibrosis[m]
Mean fluorescence intensity value		g3, ptc3, i1, t0, v0,	g0, ptc1, i1, t0, v),
		cg3, cptc0, ci2, ct2, C4d-	cg0, cptc0, ci0, ct0, C4d-
		Not detected	Detected
		Class I – 0	Class I – 1839 against Cw5
		Class II – 0	Class II – 10512 against DQ4

Clinical Information	Kidney Biopsies[a]		
	Native Kidney [HK][b]	Allograft Kidney #1 [AK1 (TG w/ graft dysfunction)][c]	Allograft Kidney #2 [AK2 (aABMR f/u)][d]
From index biopsy to last follow up[h]	12 months	12 months	12 months
Time, index biopsy to last follow up	1.14	Graft failure, Initiated on dialysis	1.64
Serum creatinine, mg/dl	21	-	0.09
Urine albumin:creatinine ratio, mg/g	Not detected	Not detected	Detected
Donor-specific anti-HLA antibodies	Class I – 0	Class I – 0	Class I – 2228 against Cw5
Mean fluorescence intensity value	Class II – 0	Class II – 0	Class II – 5361 against DQ4
Maintenance immunosuppression	Tacrolimus/Mycophenolate	None	Tacrolimus/Mycophenolate/Prednisone

[a]:Biopsies were evaluated by light, immunofluorescence and electron microscopy. Sections were stained with hematoxylin and eosin, periodic acid–Schiff, Masson trichrome, as well as for polyomavirus, immunoglobulins, complement proteins including complement factor 4 degradation product d (C4d). Each patient provided a single biopsy sample for this study. All three biopsies were done using an 18 g size Bard® Monopty® disposable core biopsy instrument (Bard Biopsy, Tempe, AZ).

[b]:Native kidney biopsy tissue (HK) was obtained from the healthy kidney donor at the time of transplantation.

[c]:Allograft kidney biopsy tissue #1 (AK1) was obtained at the time of core needle biopsy of the allograft. In an earlier biopsy, chronic tissue injury and remodeling characterized by glomerular capillary basement membrane duplication (transplant glomerulopathy [TG]) was observed. Transplant glomerulopathy represents a form of chronic immune rejection likely mediated by circulating antibodies predominantly directed against the donor HLA. However, circulating IgG antibodies directed against the donor HLA prior to transplant or at any time in the post-transplant period were not detected using the highly sensitive single antigen bead assay. We did not test for non-HLA antibodies. Biopsy AK1 was done for worsening serum creatinine and proteinuria.

[d]:Allograft kidney biopsy tissue #2 (AK2) was obtained at the time of core needle biopsy of the allograft. In an earlier biopsy, active antibody-mediated rejection (aABMR), characterized histologically by inflammation of the microvasculature in the kidney and likely mediated by circulating antibodies predominantly directed against the donor HLA was observed. Kidney allograft dysfunction associated with active AMR was successfully reversed and Biopsy AK2 was done for surveillance purpose.

[e]:Complement-dependent cytotoxicity.

[f]:Flow cytometric cross match was positive for both recipient B cells (auto flow cytometry crossmatch) and kidney donor B cells (donor flow cytometry crossmatch).

[g]:Circulating immunoglobulin G antibodies in the transplant recipient directed against one or more donor HLA were measured using the highly sensitive single antigen bead assay on a Luminex platform. Mean fluorescence intensity is a measure of the degree of saturation of target antigens present on a single bead by antibodies and is used as a surrogate for the level of antibody titers. A mean fluorescence intensity value of ≥2000 is considered positive for the presence of antibodies.

[h]:The index biopsy was the kidney allograft biopsy tissue sample used for scRNA-seq.

[i]:The prior biopsy in the 51 years old female recipient had transplant glomerulopathy (chronic glomerulopathy [cg] score > 0) and microvascular inflammation but did not fulfil the Banff criteria for antibody-mediated rejection.

[j]:The prior biopsy in the 29 years old male recipient was categorized as active antibody-mediated rejection, based on microvascular inflammation (MVI), positive peritubular capillary staining for complement split product 4d (C4d), and the presence of circulating antibodies directed against the donor HLA (DSA).

[k]:Biopsies were reported—based on the Banff 2017 update of the Banff '97 classification of allograft pathology[1]—independently by two transplant pathologists at our center who were blinded to the sequencing data.

[l]:The index biopsy in the 51 years old female recipient had severe transplant glomerulopathy (chronic glomerulopathy [cg] score > 0) and severe microvascular inflammation but did not fulfil the Banff criteria for chronic active antibody-mediated rejection.

Clinical Information	Kidney Biopsies[a]		
	Native Kidney	Allograft Kidney #1	Allograft Kidney #2
	[HK][b]	[AK1 (TG w/ graft dysfunction)][c]	[AK2 (aABMR f/u)][d]

[m]:The index biopsy in the 29 years old male recipient had mild microvascular inflammation and did not fulfil the criteria for active antibody mediated rejection.

Biopsy AK1 was obtained by ultrasound guidance from a 51-year old woman. She developed end-stage kidney disease due to lupus nephritis and received a living-donor kidney transplant. She had worsening of proteinuria after the living-donor kidney transplantation and an allograft biopsy 26 months after transplantation revealed microvascular inflammation and transplant glomerulopathy. The biopsy, however, did not fulfill the Banff criteria (an international standardized criteria for reporting allograft biopsies) for antibody-mediated rejection and there was no evidence for recurrence of lupus nephritis. Circulating immunoglobulin G antibodies directed against the donor HLA prior to transplant or at any time in the post-transplant period were not detected using the highly sensitive single-antigen bead assay. We did not test for non-HLA antibodies. Before transplant, she had a negative T and B cell complement-dependent cytotoxicity cross match and a negative T cell flowcytometry crossmatch. However, she had a positive B cell flowcytometry crossmatch to her kidney donor cells (donor flow cytometry B cell crossmatch) and to her own cells (auto flow cytometry B cell crossmatch). The index biopsy that was used for scRNA-seq was done for worsening proteinuria and kidney function 16 months after the initial biopsy.

Biopsy AK2 was obtained by ultrasound guidance from a 29-year old man. He had end stage kidney disease due to focal and segmental glomerulosclerosis. He developed acute elevation of serum creatinine, 76 months after a living-donor kidney transplantation and allograft biopsy revealed active antibody-mediated rejection (Banff category 2) with no chronic glomerular or tubulointerstitial changes. He was treated with our transplant center protocol comprised of methylprednisolone, plasmapheresis, intravenous immunoglobulin, and bortezomib and had resolution of graft dysfunction. The index biopsy that was used for scRNA-seq was done by the treating physician for surveillance purpose 8 months after the acute rejection episode. Subject AK2 had normal/stable graft function (serum creatinine < 2 mg/dl and albuminuria < 500 mg/day) at the time of the index biopsy but had persistent circulating IgG antibodies directed against the donor HLA.

Identification of distinct cell types in healthy and allograft kidneys

We conducted iterative cell clustering analysis using Seurat V3.1, an R package for exploration of single-cell data. We obtained 9762 cells; 2545 cells with > 25% mitochondrial content were removed from subsequent analysis. The final single-cell gene expression matrices for the three kidney biopsies were comprised of 7217 high-quality cells and separated into 12 cell clusters by gene expression (Fig. 1A, left) with no contributions from batch processing (Fig. 1A, right). Based on differential gene expression and previously established markers of cell types or states we designated these clusters as proximal tubular cells (PT1 and PT2), tubular progenitor cells (PG), cluster of loop of Henle cells, collecting duct cells, and intercalated cells (LH.CD.IC), fibroblasts (FB), endothelial cells (EC), cluster of pericytes and vascular smooth muscle cells (PC.vSMC), T cells (TC), natural killer cells (NK), cluster of B cells and plasma cells (BC.PLASMA), cluster of macrophages and dendritic cells (MAC.DC), and monocytes (MONO) (Fig. 1B and Table S1). During subclustering analysis, we removed 113 endothelial cell and pericyte doublets as well as 26 epithelial and T cell doublet.

Sex differences between kidney recipient and donor reveal migratory graft infiltrating cells

AK1 was a female recipient of a kidney from a male donor and AK2 was a male recipient of a kidney from a female donor. We took advantage of the sex mismatch between kidney recipients and their donors and monitored the expression of male-specific Y chromosome-encoded EIF1AY and DDX3Y and female-specific XIST, involved in female X chromosome inactivation, to determine recipient or donor origin of the cells in the allograft [12]. We first separated the cell clusters by individual samples and then assigned each cluster to either female or male origin based on the expression pattern of XIST, EIF1AY, and DDX3Y genes. Overall, the frequency for capture of sex-specific transcripts was higher for female cells as XIST was more abundant in expression compared to EIF1AY and DDX3Y. HK kidney was obtained from a female kidney donor and as expected, the cell clusters expressed XIST and lacked in expression of EIF1AY and DDX3Y, indicating their female origin (Fig. 1C).

In accord with AK1 being a female recipient of male kidney, the graft infiltrating immune cell types TC, NK, BC.PLASMA, and MAC.DC were of female origin and matched the sex of the allograft recipient. In accord with AK2 being a male recipient of female kidney, the graft infiltrating immune cell types were of male origin and also matched the sex of the recipient. In contrast to the infiltrating cells, the AK1 kidney parenchymal cells were male and matched the sex of the organ donor, while AK2 kidney parenchymal cells were female but also matched the donor. The female-specific expression of XIST was not consistent across all non-migratory cell types as exemplified by its absence in PT1 and PT2 of AK2 and HK female kidneys.

Unexpectedly, the majority of the FBs identified in AK1 were of recipient origin (like the immune cells), indicating that these FBs are migratory in nature and their presence in the allograft is by infiltration of cells from the recipient (Table S2). The AK1 kidney biopsy had a Banff chronic lesion score of 2 for interstitial fibrosis (ci score), defined by interstitial fibrosis involving 26–50% of cortical area. This finding is particularly striking considering that FBs in AK2, where the biopsy had a Banff ci score of 0, defined by interstitial fibrosis involving ≤5% of cortical area, were all matching the donor (like the kidney parenchymal cells) and not the recipient.

Comparative analysis of fibroblast-specific gene expression in healthy and allograft kidneys

To further resolve the FB cluster, we performed subclustering analysis, which separated FBs into four distinct subpopulations (FB1-4) (Fig. 2A, top panel), all of which expressed the canonical fibroblast marker DCN (Fig. 2B). FB1 was mostly comprised of fibroblasts from AK1 whereas FB2 and FB3 were predominantly from HK (Fig. 2A, bottom panel). Interestingly, FB4 were from both AK1 and AK2. FB1 cells from AK1 were exclusively of the recipient sex whereas FB4 cells from AK1 and AK2 matched their donor sex. Overall, the gene expression signature of the FB1 was similar to the FB2 cells whereas the FB3 profile was similar to the FB4 cells. FB3 and FB4 co-expressed GGT5 and EMILIN1, markers recently reported in healthy kidney biopsy to represent interstitial fibroblasts [13]. In addition, these FBs expressed ACTA2, indicative of myofibroblast-like characteristics [14]. FB1 and FB2 showed expression of the secretory factors CFD, SFRP2 and SFRP4 in addition to MFAP5, S100A4 and S100A10, the latter of which represent genes implicated to promote cell migration [15]. The infiltrating FB1 cells uniquely expressed FBN1, IFI27, WISP2 and PLA2G2A. FB4 cells uniquely expressed TNC, COL4A1, COL18A1, and TGM2, genes involved in beta-1 integrin cell surface interactions and cell adhesion to the extracellular matrix, included cellular stress response (JUN, FOSB), frequently observed in single-cell analysis and likely caused by cell dissociation [16]. Furthermore, FB1 cells did not express lineage markers of any other identified cell type and therefore cannot be considered cell doublets (Figure S1).

Tubular progenitor cell populations are increased in allograft kidneys

Combined subclustering analysis of the epithelial cells of PT1-2, PG, and LH.CD.IC resolved into 6 subpopulations (Fig. 3A-B). Proximal tubular cells (PT) were marked by expression of MIOX, ANPEP, and SLC13A1 genes (Fig. 3C). The two groups of PGs—major (PG1) and minor (PG2)—were defined as $PROM1^{+}CD24^{+}VIM^{+}$ cells but with distinct differences (Figure S2). PGs lack brush border, are shown to be scattered throughout the proximal tubule in the normal kidney and become more numerous and participate in tubular regeneration after acute tubular injury [17,18]. Interestingly, PGs also specifically expressed CDH2 (N-cadherin), a known marker for epithelial-mesenchymal transition (EMT) [19]. The co-expression of proximal tubular cell marker genes in PG1 suggests a more differentiated state compared to PG2. Although PGs were present in all three samples, AK1 contributed more than half of them (PG1 79.3% and PG2 55%) (Fig. 3D).

The key histological feature of AK1 kidney was interstitial fibrosis. To examine whether PG abundance and gene expression contributed to the fibrotic characteristic, we performed matrisome (the ensemble of extracellular matrix (ECM) and ECM-associated proteins) enrichment analysis [20,21] of PT and PG subtypes (Fig. 3E). Most of the expressed collagen genes including COL4A1, COL4A2, and COL1A1, were selectively enriched in PGs and showed no or minimal expression in PT cells. Similarly, the second category of matrisome genes 'proteoglycans' also showed enrichment in PGs and not in PT. In addition, the secreted factors including S100A family genes and cytokines such as CCL2, CXCL1, and CXCL6 were abundant in PGs. The other epithelial cells of the kidney such as LH, CD, and IC-A were identified by unique expression of marker genes UMOD, AQP2, and ATP6V0D2, respectively.

Subclustering analysis of the endothelial cells identify active population

Further investigation into endothelial cell gene expression revealed four distinct subtypes; AVR1-3 and descending vasa recta (DVR), primarily based on the expression of PLVAP, AQP1, and SLC14A (Fig. 4A-B). Glomerular endothelial cells were not captured, although some ECs expressed markers classified as glomerular endothelial markers, but their contribution was insufficient to separate into a distinct cell cluster. All EC subclusters shared expression of canonical markers such as PECAM1 and CDH5. The AVR2 subpopulation, mostly composed of AK2 cells, was characterized by unique expression of group the structurally and functionally related cytokines CXCL9, CXCL10, and CXCL11 (Fig. 4A-C). These cytokines act as chemoattractants during inflammation through binding to the receptor CXCR3 mostly expressed by activated T cells [22]. AK1 and AK2 AVR showed > 6-fold upregulation of the cell-surface-glycoprotein-encoding SELE gene compared to HK (SELE TPM, HK: 0.6, AK1: 2.6, AK2: 4.1). Under inflammatory conditions, endothelial cells induce expression of SELE in order to facilitate trans-endothelial passage of leukocytes through adhesion to the vascular lining [23]. The AVR3 subpopulation showed higher expression of JUN, FOS and JUNB and likely represent stressed cells induced during the sample processing (Figure S3).

Pericytes and vascular smooth muscle subtypes in the kidney

The vascular smooth muscle cell and pericyte cluster resolved into six subpopulations: vSMC1-4 and PC1-2 (Fig. 4D and S4). vSMC1-2, mostly comprised of HK cells, showed abundant expression of stress induced genes (relatively more in vSMC1 than vSMC2) such as JUNB and FOSB

(Fig. 4E). Interestingly, the allograft vSMC3-4, composed of AK1 and AK2 cells respectively, differentiated from the healthy vSMC1-2 (mostly HK cells) by expression of cardiac muscle alpha actin (ACTC1) gene indicating its expression is likely induced due to inflammation. Upregulation of NNMT, considered as master metabolic regulator and contributing to secretion of cytokines and oncogenic extracellular matrix of cancer-associated fibroblasts [24]. The AK1 allograft with high interstitial fibrosis showed exclusive expression of NNMT in the vSMC3 and AVR cells. The two subpopulations, vSMC3 and vSMC4 were distinguished only by two genes, EIF1AY and NNMT, and likely represent the same cell type. Higher level of stress response genes JUNB and FOSB separated PC1 from PC2. In addition, PC2 cells expressed THY1, S100A4, and CCL2 genes and exclusively originated from HK cells.

Immune cell heterogeneity in the healthy and allograft kidneys

Subclustering analysis of the immune cell populations further resolved TC, cytotoxic TC, NK, MONO, MAC, DC, BC, PLASMA, and MAST (mast cells) clusters (Fig. 5A-C). As anticipated, AK1 and AK2 showed higher proportions of immune cell infiltrates (52% and 66%, respectively, vs. 16% of all cells) (Fig. 5D). The T cells in HK were dominated by granzyme-K- (GZMK-) producing $CD8^+$ T cells, and a small subset of interferon-stimulated-gene- (ISG-) high $CD4^+$ T cells with increased expression of ISG15, MX1, RSAD2, IFIT1, and IFIT2 (Fig. 5E). ISG-high $CD4^+$ T cells were also found in AK1 and AK2. Furthermore, AK2 showed a large subpopulation of GZMK-expressing $CD8^+$ cytotoxic T cells, and a smaller subgroup of $CD8^+$ cytotoxic T cells, defined by high expression of granzyme B (GZMB) and perforin (PRF1). We also identified a minor population of central memory T cells in AK2 characterized by expression of CCR7, SELL, and TCF7. MAC expressed MS4A4A, STAB1 and SEPP1 typically considered as gene signatures of “alternatively activated” M2 macrophages. The proportion of NK and MONO cells in AK1 (0.38% and 0.44%, respectively) compared to AK2 (9.8% and 7.8%, respectively) was remarkably reduced. Interestingly, while only one PLASMA cell was detected in AK1, these cells made about 1.5% percent of total cells in AK2 sample. IRF1 was ≥ 10-fold abundant in MACs of AK2 (TPM 3.1) compared to AK1 (TPM 0.3) and HK (TPM 0.1). IRF1 mRNA was also increased in cytotoxic TCs of AK2 (TPM 3.0) compared with AK1 (TPM 1.7) and HK (TPM 1.4). Given their small number, the biological relevance of immune cell heterogeneity should be interpreted with caution.

Discussion

The key findings of our single-cell transcriptome analysis include: (i) allograft kidney biopsy AK1, with ongoing tubulointerstitial fibrosis, contained recipient-derived fibroblasts in contrast to the allograft kidney AK2 biopsy with no fibrosis and exclusively donor-derived FBs; (ii) allograft kidney AK1 biopsy also contained proximal tubular progenitor cells that were enriched in the expression of ECM glycoproteins, collagens, and proteoglycans, and (iii) allograft kidney AK2 biopsy, eight months after successful treatment of antibody-mediated rejection as defined by clinical and histological criteria, contained endothelial cells expressing T cell chemoattractant cytokines. Determining the frequency of these observations is essential and will require scRNA-seq studies on larger cohorts of similar phenotype.

The discovery of migratory recipient-derived fibroblast subtypes in a human allograft kidney biopsy is prompting for the investigation of molecular cues leading into recruitment of such migratory FBs to the kidney, the answer of which may hold immense therapeutic implications. The AK1 biopsy showed chronic parenchymal injury and graft dysfunction and manifested histologically as TG and interstitial fibrosis. Recent studies in animal models have demonstrated that bone-marrow-derived FBs contribute significantly to kidney fibrosis [25]. However, there is controversy on the relative contribution of different cell types including FBs, fibrocytes, pericytes, bone marrow-derived FBs, epithelial cells, and endothelial cells to myofibroblast differentiation and extracellular matrix deposition in kidney fibrosis [26]. Our observation suggests that the migratory and tissue-invasive nature of the FBs unique to the AK1 biopsy may play a crucial role in fibrosis and complements the prior observation of mesenchymal cells of host origin in the vascular and interstitial compartments of kidney allografts undergoing chronic rejection [27]. The migratory FB1 and non-migratory FB4 subpopulation identified in the AK1 biopsy were differentiated by MFAP5 and S100A4 expression in the migratory FBs. Increased stromal MFAP5 was reported to stimulate cancer cell motility and invasion and predicted poor survival, and MFAP5 in vivo silencing reduced tumor progression [15]. Calcium-binding protein S100A4 promotes metastasis and is associated with intestinal fibroblast migration in patients with Crohn’s disease [28,29]. The discovery of FBs expressing MFAP5 and S100A4 in healthy kidney suggests that our findings provide unique opportunities for targeting FBs in order to ameliorate interstitial fibrosis.

PROM1 (CD133) positive tubular progenitor cells co-expressing ECM glycoproteins, collagens, and proteoglycans in AK1 biopsy with interstitial fibrosis and tubular atrophy is a novel finding. While the contribution of EMT to kidney fibrosis is a subject of considerable controversy, recent evidence suggests that partial EMT is sufficient to induce the release of fibrogenic cytokines [30]. Our detection of tubular PG cells, but not other tubular epithelial cells, expressing CDH2 (N-cadherin) suggests partial EMT in PGs. Though these cells expressed tubular cell markers, they could not be categorized as distinct tubular cell subsets. The PGs expressed several S100 proteins, a family of calcium-binding proteins involved in cell apoptosis, migration, proliferation, differentiation, energy metabolism, and inflammation. In human kidneys, $PROM1^+$ cells have been found distributed throughout the kidney and are capable of expansion and limited self-renewal [31]. Identifying partial EMT in tubular progenitor cells rekindles the role of tubular cells in perpetuating fibrosis.

In AK2 biopsy, a subpopulation of endothelial cells expressed mRNA for cytokines CXCL9, CXCL10 and CXCL11 while T cells expressed the cognate receptor CXCR3. Such communication of endothelial cells through T cell chemoattractant, eight months after successful treatment of antibody-mediated rejection, is striking and highlights the role of endothelium in perpetuating tissue injury in the presence of circulating antibodies directed against the donor HLA, despite the clinical success achieved with treating the rejection episode. Endothelium as a source of CXCL10 was previously noted in a cardiac allograft model and initiation of alloresponses [32].

A strength of our study, despite its limited sample number, is the rapid processing of freshly collected biopsies without cryopreservation, albeit on different days. We minimized the time for transfer of the samples from the ultrasound suite or the operating room, where the biopsies were performed, to the research laboratory for generating single-cell suspensions, and from the research laboratory to the genomics core laboratory for library preparation. We used the 10x Chromium platform (10x Genomics) with high cell-capture efficiency and permitting the use of human kidney allograft biopsies with limiting amount of tissue [6]. Earlier reports on scRNA-seq of healthy and diseased human kidney tissue, both native and allograft kidney, have included a combination of single-cell and single-nucleus sequencing [14], fresh and frozen specimens [33], multiple platforms to capture the single cells [14,34] and analyzing the transcriptome after pooling cells from multiple samples [35]. Another strength is the use of normal kidney tissue from a living kidney donor, instead of unaffected areas of tumor nephrectomies or kidneys rejected for transplantation.

Our study has limitations. The number of study subjects was sparse, and we analyzed only three biopsies. Our findings need to be validated in more biopsies. Extrapolating from these results is challenging because of the heterogeneity in rejection and tissue sampling depth by core needle biopsy. However, having implemented a standardized protocol for sample preparation, single-cell capture, RNA-seq, and data analysis, we believe that—despite limited number of samples—our results are robust and have provided rich mechanistic information. Another limitation is that not every cell type is captured by our whole cell dissociation protocol, in particular podocytes. Nevertheless, we were able to capture and analyze several glomerular cell types including the parenchymal cells; continued refinement of tissue processing techniques is expected to further improve the types of cells captured. Finally, there are inherent limitations to the scRNA-seq technique, for example, only a fraction of mRNAs present in cells are captured and converted to cDNA and the tissue dissociation process disrupts tissue architecture and loses relative spatial positioning information of cells.

In summary, we have demonstrated the utility of scRNA-seq in interrogating intragraft events in kidney allografts. Our analysis has revealed unique cell types and cell states in kidney allograft biopsies and confirmed our hypothesis that applying scRNA-seq furthers precision transplantation medicine approaches by providing mechanistic insights and opportunities for drug target and pathway identification at hitherto unknown and unavailable resolution. With improvement in the technology, refinement in computational approaches, and decreasing operational costs, it is possible in the future to apply single-cell transcriptomics to complement conventional histopathology, in the clinic, for the idealized care of transplant recipients.

Methods

Tissue collection, dissociation, and single-cell preparation

At the time of needle biopsy, a core of the biopsy tissue was earmarked for single-cell preparation and was transported in phosphate-buffered saline immediately to our Gene Expression Monitoring laboratory and were immediately dissociated for single-cell capture. We developed and used an in-house protocol for single-cell preparation. In brief, the sample was placed in 400 µl of freshly prepared tissue dissociation solution comprised of 100 µl Liberase TL solution (2 mg/ml, Sigma-Aldrich), 500 µl Tyrode's solution-HEPES-based (Boston BioProducts), and 200 µl DNase I solution (1 mg/ml, Stemcell technologies) and incubated at 37ºC water bath for 15 min. The cell suspension was passed through a 40 µm Falcon™ cell strainer (ThermoFisher Scientific) into a 50 ml centrifuge tube filled with 5 ml fetal bovine serum (ThermoFisher Scientific), washed through with Dulbecco's phosphate-buffered saline (ThermoFisher Scientific), and centrifuged for 5 min at 300 g. Cells were resuspended in 2% bovine serum albumin (New England BioLabs) and were transferred immediately in ice to the genomics core laboratory.

Single-cell capture, library preparation, sequencing, data processing, and generation of gene expression matrix

Single-cell suspension on ice was immediately transferred to the Weill Cornell Medicine genomics core facility. scRNA-seq libraries were prepared using the Chromium Single Cell 3' Reagent Kit V2 (10x Genomics) according to the manufacturer's instructions. The library was sequenced on Illumina HiSeq 2500 platform as follows: 26 bp (Read1) and 98 bp (Read2). The sequencing was performed to obtain 150–200 million reads (each for Read1 and Read2). The 10x raw data were processed individually for 3 kidney samples using previously described Drop-seq pipeline (Drop-seq core computational protocol V1.2, http://mccarrolllab.com/dropseq/) with the following parameters. The Read1 bases 1–16 were tagged with cell barcode 'XC' and bases 17–26 were tagged with a unique molecular identifier (UMI) 'XM'. Low-quality bases containing reads were removed and the 3'-end of Read2 was trimmed to remove poly(A) sequences of six or more bases and were aligned to

human genome (hg38) reference using STAR aligner (STAR_2.5.1a), allowing no more than three mismatches. The gene expression matrix was then generated using the 'MIN_BC_READ_THRESHOLD = 2' option to retain UMIs with read evidence of two or more.

scRNA-seq data analysis

Cell clustering analysis was performed collectively for all 3 samples using Seurat V3.1, an R package for exploration of single-cell data. Briefly, only those genes that were expressed in more than three cells and cells that expressed more than 200 but less than 5000 genes were retained. Ubiquitously expressed genes such as ribosomal protein-coding (RPS and RPL) and non-coding RNA (MALAT1) genes were removed. We also removed miRNA and snoRNA genes from clustering analysis. The clustering analysis was performed in an iterative manner where in round 1 the cells with > 25% mitochondrial content was identified and removed from round 2 clustering analysis. In round 2 analysis, mitochondrially coded genes (MT-) were also dropped from clustering analysis. Next, we separated endothelial cells, epithelial cells, immune cells and stromal cells into their individual Seurat objects and conducted at least two rounds of analysis on each to identify and remove doublet captures. Typically, doublet capture show expression of markers of two different lineages (e.g., T cells and epithelial cells). Using function 'FindVariableFeatures' ~2000 genes were identified, followed by 'ScaleData'. Next, 'RunPCA', 'FindNeighbors', 'FindClusters', and 'RunUMAP' was used with different dimensions 1:10 and resolution of 0.5 wherever these options were needed. Reduction method "umap" was used and clusters were plotted using 'DimPlot' option. To identify differentially expressed genes by each cluster, Wilcoxon rank sum test inbuilt in the Seurat package was used with parameters 'min.pct = 0.25' and 'thresh.use = 0.25'.

Subclustering analyses of the cell groups described in this manuscript were performed using similar strategy as described above. The expression of established lineage marker genes was used to assign cell types. Once the cell types were identified, average expression was calculated followed by normalization to 10,000 to create a TPM (transcript per million)-like value. For the 'donor/recipient origin of cells' analysis, separate Seurat objects were created for HK, AK1, and AK2 cells maintaining the original cell type identity. Using 'DotPlot' function, expression of female (XIST) and male (EIF1AY, DDX3Y)-specific genes was plotted.

For cells of the ascending vasa recta (AVR), in order to perform differential gene expression analysis by samples, we could not employ the conventional differential gene expression analysis methods such as DESeq2 or edgeR, due to the small number of samples. For this analysis, we only allowed genes that had > 2 TPM expression in at least one of the samples (HK, AK1, or AK2). Next, for each gene, we calculated the largest (maximal) and second largest TPM expression values across all three samples. Finally, only the genes with at least two-fold difference between maximal and second largest TPM were reported.

Matrisome enrichment analysis

Normalized expression profiles of PT, PG1 and PG2 were generated and used for matrisome analysis. We utilized a previously described list of matrisome genes and then subset the list for each category of matrisomes (collagen, proteoglycan, and secreted factor) from the TPM expression profiles of PT, PG1, and PG2 cell types. $Log_2(TPM + 1)$ values for top expressed genes in each of the matrisome category were represented in the heatmap.

Study approval

The clinical and research activities that we report here are consistent with the principles of the "Declaration of Istanbul on Organ Trafficking and Transplant Tourism"[36]. The research protocol was approved by the Weill Cornell Medicine Institutional Review Board (protocol number: 1404015008). The transplant recipients reported herein provided written informed consent to participate in the study and the informed consent was obtained prior to their inclusion in the study.

Declarations

STATEMENT ON DATA AVAILABILITY

Further information and requests for resources should be directed to and will be fulfilled by the corresponding author, Thangamani Muthukumar (mut9002@med.cornell.edu). This study did not generate new unique reagents. The scRNA-seq data files have been deposited at NCBI's Gene Expression Omnibus under the accession number GSE151671.

ACKNOWLEDGEMENTS

Supported in part by awards from the National Institutes of Health (NIH MERIT Award, R37-AI051652 to M. Suthanthiran, K08-DK087824 and R03-DK105270 to T. Muthukumar, and NCATS Clinical and Translational Science Award, UL1TR000457 to Weill Cornell Medical College) and an award from the Mendez National Institute of Transplantation Foundation to M. Suthanthiran. We thank ThuTrang Du, Division Administrator, Division of Nephrology, Weill Cornell Medical College, for her help with the execution of this project. We thank A. Hurley and the

Research Facilitation Office staff at Rockefeller University, supported in part by the NCATS Clinical and Translational Science Award, UL1TR001866 to the Rockefeller University from the NIH, for their regulatory and administrative assistance.

AUTHOR CONTRIBUTIONS

Designed research: H.S., H.Y., M.S., T.M.

Conducting experiments: H.Y., M.L., A.A., C.L., C.S., V.K.S., T.M.

Acquiring data: H.S., H.Y., M.L., A.A., F.B.M., J.R.L., D.M.D., S.P.S., S.V.S., T.T., T.M.

Analyzing data: H.S., M.L., P.M., S.V.S., T.M.

Providing reagents: S.V.S., T.T., M.S.

Writing the manuscript: H.S., T.T., M.S., T.M.

STATEMENT ON COMPETING INTERESTS

The authors declare no competing interests

References

1. Haas, M. *et al.* The Banff 2017 Kidney Meeting Report: Revised diagnostic criteria for chronic active T cell-mediated rejection, antibody-mediated rejection, and prospects for integrative endpoints for next-generation clinical trials. *Am J Transplant.* **18**, 293–307 https://doi.org/10.1111/ajt.14625 (2018).
2. Naesens, M. & Anglicheau, D. Precision Transplant Medicine: Biomarkers to the Rescue. *J Am Soc Nephrol.* **29**, 24–34 https://doi.org/10.1681/ASN.2017010004 (2018).
3. Loupy, A. *et al.* The Banff 2015 Kidney Meeting Report: Current Challenges in Rejection Classification and Prospects for Adopting Molecular Pathology. *Am J Transplant.* **17**, 28–41 https://doi.org/10.1111/ajt.14107 (2017).
4. Varma, E., Luo, X. & Muthukumar, T. Dissecting the human kidney allograft transcriptome: single-cell RNA sequencing. *Curr Opin Organ Transplant.* https://doi.org/10.1097/MOT.0000000000000840 (2020).
5. Malone, A. F. & Humphreys, B. D. Single-cell Transcriptomics and Solid Organ Transplantation. *Transplantation.* **103**, 1776–1782 https://doi.org/10.1097/TP.0000000000002725 (2019).
6. Malone, A. F., Wu, H. & Humphreys, B. D. Bringing Renal Biopsy Interpretation Into the Molecular Age With Single-Cell RNA Sequencing. *Semin Nephrol.* **38**, 31–39 https://doi.org/10.1016/j.semnephrol.2017.09.005 (2018).
7. Alkadi, M. M. *et al.* Kidney allograft failure in the steroid-free immunosuppression era: A matched case-control study. *Clin Transplant.* **31**, https://doi.org/10.1111/ctr.13117 (2017).
8. Clayton, P. A., McDonald, S. P., Russ, G. R. & Chadban, S. J. Long-Term Outcomes after Acute Rejection in Kidney Transplant Recipients: An ANZDATA Analysis. *J Am Soc Nephrol.* https://doi.org/10.1681/ASN.2018111101 (2019).
9. Cole, E. H., Johnston, O., Rose, C. L. & Gill, J. S. Impact of acute rejection and new-onset diabetes on long-term transplant graft and patient survival. *Clin J Am Soc Nephrol.* **3**, 814–821 https://doi.org/10.2215/CJN.04681107 (2008).
10. Hart, A. *et al.* OPTN/SRTR 2017 Annual Data Report: Kidney. *Am J Transplant.* **19 Suppl 2**, 19–123 https://doi.org/10.1111/ajt.15274 (2019).
11. El Ters, M. *et al.* Kidney allograft survival after acute rejection, the value of follow-up biopsies. *Am J Transplant.* **13**, 2334–2341 https://doi.org/10.1111/ajt.12370 (2013).
12. Butler, A., Hoffman, P., Smibert, P., Papalexi, E. & Satija, R. Integrating single-cell transcriptomic data across different conditions, technologies, and species. *Nat Biotechnol.* **36**, 411–420 https://doi.org/10.1038/nbt.4096 (2018).
13. Suryawanshi, H. *et al.* A single-cell survey of the human first-trimester placenta and decidua. *Sci Adv.* **4**, eaau4788 https://doi.org/10.1126/sciadv.aau4788 (2018).
14. Wu, H. *et al.* Single-Cell Transcriptomics of a Human Kidney Allograft Biopsy Specimen Defines a Diverse Inflammatory Response. *J Am Soc Nephrol.* **29**, 2069–2080 https://doi.org/10.1681/ASN.2018020125 (2018).
15. Leung, C. S. *et al.* Calcium-dependent FAK/CREB/TNNC1 signalling mediates the effect of stromal MFAP5 on ovarian cancer metastatic potential. *Nat Commun.* **5**, 5092 https://doi.org/10.1038/ncomms6092 (2014).

16. van den Brink, S. C. *et al.* Single-cell sequencing reveals dissociation-induced gene expression in tissue subpopulations. *Nat Methods.* **14**, 935–936 https://doi.org/10.1038/nmeth.4437 (2017).
17. Smeets, B. *et al.* Proximal tubular cells contain a phenotypically distinct, scattered cell population involved in tubular regeneration. *J Pathol.* **229**, 645–659 https://doi.org/10.1002/path.4125 (2013).
18. Lindgren, D. *et al.* Isolation and characterization of progenitor-like cells from human renal proximal tubules. *Am J Pathol.* **178**, 828–837 https://doi.org/10.1016/j.ajpath.2010.10.026 (2011).
19. Wheelock, M. J., Shintani, Y., Maeda, M., Fukumoto, Y. & Johnson, K. R. Cadherin switching. *J Cell Sci.* **121**, 727–735 https://doi.org/10.1242/jcs.000455 (2008).
20. Hynes, R. O. & Naba, A. Overview of the matrisome–an inventory of extracellular matrix constituents and functions. *Cold Spring Harb Perspect Biol.* **4**, a004903 https://doi.org/10.1101/cshperspect.a004903 (2012).
21. Suryawanshi, H. *et al.* Cell atlas of the fetal human heart and implications for autoimmune-mediated congenital heart block. *Cardiovasc Res.* https://doi.org/10.1093/cvr/cvz257 (2019).
22. Panzer, U. *et al.* Compartment-specific expression and function of the chemokine IP-10/CXCL10 in a model of renal endothelial microvascular injury. *J Am Soc Nephrol.* **17**, 454–464 https://doi.org/10.1681/ASN.2005040364 (2006).
23. Silva, M., Videira, P. A. & Sackstein, R. E-Selectin Ligands in the Human Mononuclear Phagocyte System: Implications for Infection, Inflammation, and Immunotherapy. *Front Immunol.* **8**, 1878 https://doi.org/10.3389/fimmu.2017.01878 (2017).
24. Eckert, M. A. *et al.* Proteomics reveals NNMT as a master metabolic regulator of cancer-associated fibroblasts. *Nature.* **569**, 723–728 https://doi.org/10.1038/s41586-019-1173-8 (2019).
25. Yan, J., Zhang, Z., Jia, L. & Wang, Y. Role of Bone Marrow-Derived Fibroblasts in Renal Fibrosis. *Front Physiol.* **7**, 61 https://doi.org/10.3389/fphys.2016.00061 (2016).
26. Sun, Y. B., Qu, X., Caruana, G. & Li, J. The origin of renal fibroblasts/myofibroblasts and the signals that trigger fibrosis. *Differentiation.* **92**, 102–107 https://doi.org/10.1016/j.diff.2016.05.008 (2016).
27. Grimm, P. C. *et al.* Neointimal and tubulointerstitial infiltration by recipient mesenchymal cells in chronic renal-allograft rejection. *N Engl J Med.* **345**, 93–97 https://doi.org/10.1056/NEJM200107123450203 (2001).
28. Boye, K. & Maelandsmo, G. M. S100A4 and metastasis: a small actor playing many roles. *Am J Pathol.* **176**, 528–535 https://doi.org/10.2353/ajpath.2010.090526 (2010).
29. Cunningham, M. F., Docherty, N. G., Burke, J. P. & O'Connell, P. R. S100A4 expression is increased in stricture fibroblasts from patients with fibrostenosing Crohn's disease and promotes intestinal fibroblast migration. *Am J Physiol Gastrointest Liver Physiol.* **299**, G457–466 https://doi.org/10.1152/ajpgi.00351.2009 (2010).
30. Liu, B. C., Tang, T. T., Lv, L. L. & Lan, H. Y. Renal tubule injury: a driving force toward chronic kidney disease. *Kidney Int.* **93**, 568–579 https://doi.org/10.1016/j.kint.2017.09.033 (2018).
31. Bussolati, B. *et al.* Isolation of renal progenitor cells from adult human kidney. *Am J Pathol.* **166**, 545–555 https://doi.org/10.1016/S0002-9440(10)62276-6 (2005).
32. Hancock, W. W. *et al.* Donor-derived IP-10 initiates development of acute allograft rejection. *J Exp Med.* **193**, 975–980 https://doi.org/10.1084/jem.193.8.975 (2001).
33. Der, E. *et al.* Tubular cell and keratinocyte single-cell transcriptomics applied to lupus nephritis reveal type I IFN and fibrosis relevant pathways. *Nat Immunol.* **20**, 915–927 https://doi.org/10.1038/s41590-019-0386-1 (2019).
34. Arazi, A. *et al.* The immune cell landscape in kidneys of patients with lupus nephritis. *Nat Immunol.* **20**, 902–914 https://doi.org/10.1038/s41590-019-0398-x (2019).
35. Stewart, B. J. *et al.* Spatiotemporal immune zonation of the human kidney. *Science.* **365**, 1461–1466 (2019).
36. International Summit on Transplant, T. & & Organ, T. The Declaration of Istanbul on Organ Trafficking and Transplant Tourism. *Clin J Am Soc Nephrol.* **3**, 1227–1231 https://doi.org/10.2215/CJN.03320708 (2008).

Figures

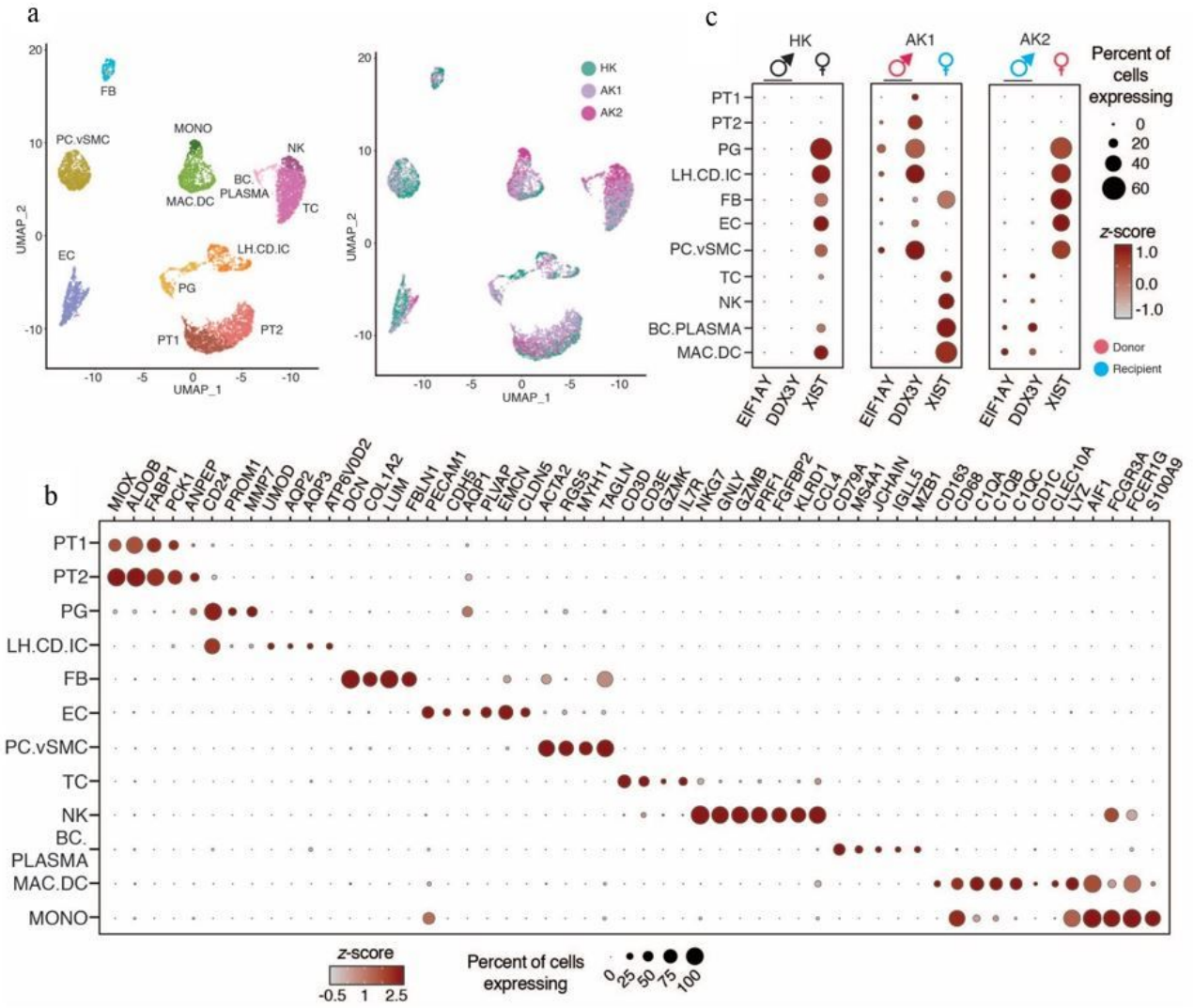

Figure 1

scRNA-seq applied to kidney allografts differentiated cell types and resolved recipient and donor origin based on sex-specific gene expression (a). Uniform manifold approximation and projection (UMAP)-based visualization of 7217 individual cells obtained from the three kidney biopsy tissues. Left Panel: UMAP-based visualization in which different clusters represent different cell types. PT1 and PT2-proximal tubular cells 1 and 2, PG-progenitor cells, LH.CD.IC-LH-cluster of loop of Henle cells, collecting duct cells, and intercalated cells, FB-fibroblasts, EC-endothelial cells, PC.vSMC-cluster of pericytes and vascular smooth muscle cells, TC-T lymphocytes, NK-natural killer cells, BC.PLASMA-cluster of B lymphocytes and plasma cells, MAC.DC-cluster of macrophages and dendritic cells, and MONO-monocytes. Right Panel: UMAP-based visualization of the same cell clusters shown in the left panel in which the cells are colored by the samples. HK-healthy kidney biopsy tissue, AK1 and AK2-allograft kidney biopsy tissues. (b). Dot-plot showing expression of known lineage markers. The size of the dot represents the proportion of cells within each cluster expressing the marker. The intensity of the color represents the standard score for each marker across different cell clusters. (c). Dot-plot showing the annotation of donor/recipient origin of cells in each sample based on female (XIST) and male (EIF1AY, DDX3Y)-specific gene expression patterns. HK is a female donor kidney; AK1 is a female recipient of a kidney from a male donor; AK2 is a male recipient of a kidney from a female donor. XIST gene produces X-inactive specific transcript (Xist) RNA, a non-coding RNA which is a major effector of the X chromosome inactivation. The Xist RNA is expressed only on the inactive chromosome and not on the active chromosome. Males (XY), who have only one X chromosome that is active, do not express it. Females (XX), who have one active and one inactive X chromosome, express it. In HK biopsy (female kidney), all the cells in the kidney express XIST and none express the Y chromosome markers. In AK1 biopsy (male donor and female recipient), all the kidney parenchymal cells express Y chromosome markers whereas all the recipient-derived immune infiltrating cells express XIST. In AK2 biopsy (female donor and male recipient), all the kidney parenchymal cells express XIST whereas all the recipient-derived immune infiltrating cells express the Y chromosome markers.

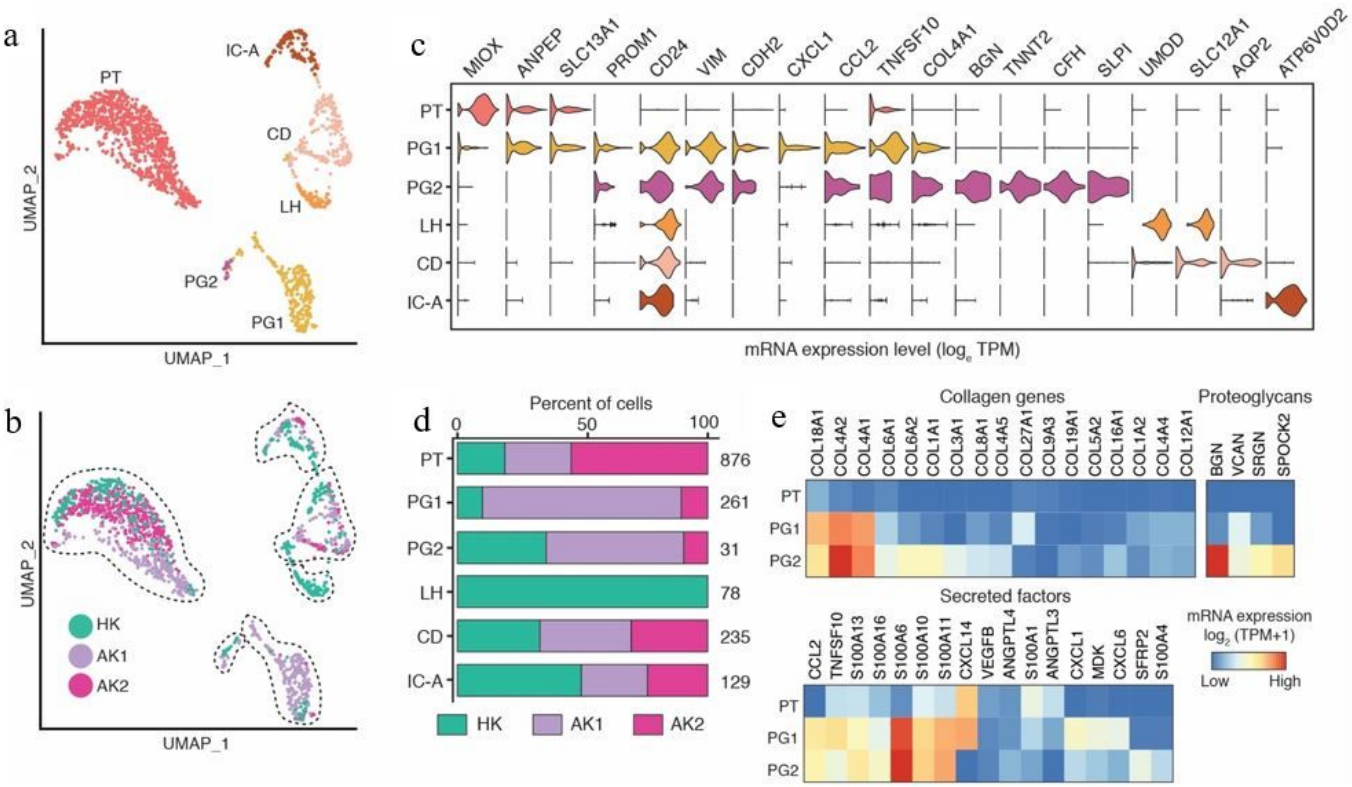

Figure 3

Epithelial cell sub-clustering revealed collagen-producing tubular progenitor cells (a). UMAP-based visualization of epithelial cells colored by different cell types. PT-proximal tubular cells, IC-A-intercalated cells type A, CD-collecting duct cells, LH-loop of Henle cells, PROG-progenitor cells. (b). UMAP-based visualization of epithelial cells colored by the biopsies HK, AK1 and AK2. (c). Violin plot showing expression of the lineage gene markers. (d). Stacked bar plots show the proportion of epithelial cells in each sample. The numbers on the right is the total number of cells. (e). Heatmap showing top expressed genes belonging to categories of matrisome groups.

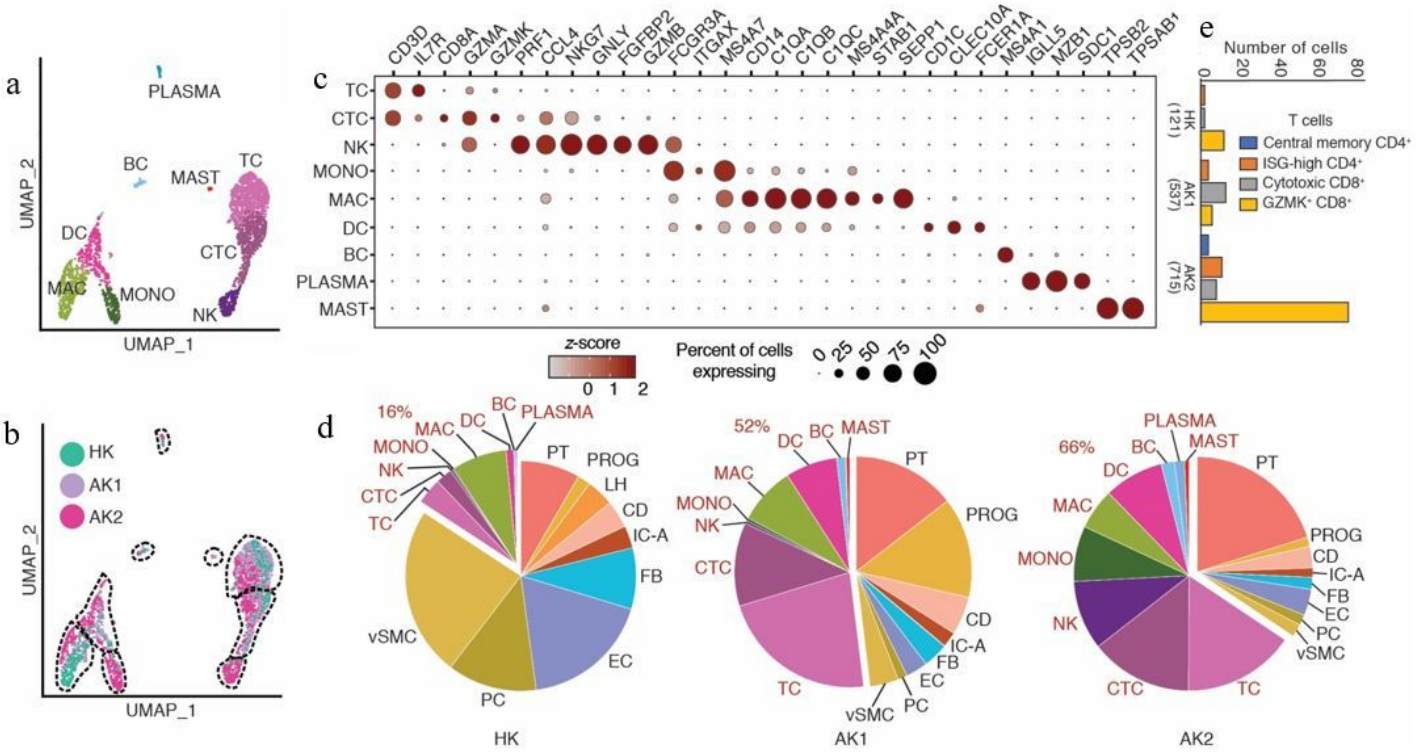

Figure 5

Immune cell heterogeneity in the healthy and allograft kidneys (a). UMAP-based visualization of immune cells colored by different cell types. TC-T lymphocytes, CTC-cytotoxic T lymphocytes, NK-natural killer cells, MONO-monocytes, MAC-macrophages, DC-dendritic cells, BC-B lymphocytes, PLASMA-plasma cells. (b). UMAP-based visualization of immune cells colored by the biopsies HK, AK1 and AK2. (c). Dot-plot showing expression of known lineage gene markers. (d). Pie chart depicting the proportion of cell types in each biopsy sample. The immune cells are labelled in red. (e). Bar graphs showing the different types of T cells in HK, AK1, and AK2. Central memory CD4+ T cells: CCR7+SELL+TCF7+, ISG-high CD4+ T cells: CD4+ISG15+, Cytotoxic CD8+ T cells: CD8A+GZMB+.

Supplementary Files

This is a list of supplementary files associated with this preprint. Click to download.

- TableS1TPM10KValues.xlsx